The effect of chemical modifications on the thermal stability of different G-quadruplex-forming oligonucleotides

Barbara Saccà, Laurent Lacroix and Jean-Louis Mergny*

Laboratoire de Biophysique, Muséum National d'Histoire Naturelle USM503, INSERM U565, CNRS UMR 5153, 43 rue Cuvier, 75231 Paris cedex 05, France

ABSTRACT

A systematic study of the thermal and conformational properties of chemically modified G-quadruplexes of different molecularities is reported. The effect of backbone charge and atom size, thymine/uracyl substitution as well as the effect of modification at the ribose 2′-position was analyzed by UV spectroscopy. Additional calorimetric studies were performed on different modified forms of the human telomeric sequence. Determination of the differential spectra allowed more insights into the conformational properties of the oligonucleotides. Lack of negative charge at the phosphate backbone yielded to a general destabilization of the G-quadruplex structure. On the other hand, substitution of thymine with uracyl resulted in a moderate or strong stabilization of the structure. Additional modification at the sugar 2′-position gave rise to different effects depending on the molecularity of the quadruplex. In particular, loss of hydrogen bond capacity at the 2′-position strongly affected the conformation of the G-quadruplex. Altogether, these results demonstrate that the effect of some modifications depends on the sequence context, thus providing helpful information for the use of chemically modified quadruplexes as therapeutic agents or as structural elements of supramolecular complexes.

INTRODUCTION

G-quadruplexes are unusual DNA structures based on the association of planar G-quartets (Figure 1a). As shown in Figure 1b, G-quadruplexes can be classified according to the number of strands that self-associate (i.e. one, two or four strands) and further differentiated by their relative orientations (parallel, anti-parallel or mixed), the orientation of the loops (lateral, diagonal or chain reversal) and the conformation of the guanine bases around the glycosidic bond (*syn* or *anti*) (1,2).

Although the basic features of G-quartets have been known for more than 40 years (3), it is only in the past decade that the level of interest in these peculiar structures has increased, due to growing evidences supporting the hypothesis of a relevant role of G-quadruplex structures in key biological processes (4–9). On the basis of these findings, some putative biological functions of G-quadruplexes have been postulated, e.g. protection of G-rich chromosomal overhangs (10,11). However, an indirect proof of their existence and role *in vivo* relies on the identification of cellular proteins that are capable of specifically recognizing such structures (12–18). In contrast, telomeric proteins, such as human telomerase, are known to bind preferentially to double-helical or single-stranded (non quadruplexed) telomeric DNA (19). Formation of G-quadruplex structures at telomeric ends of chromosomal DNA and their stabilization by specific ligands has been shown to inhibit telomerase activity in cancer cells (20–22).

In addition to the use of G-quadruplex structures as targets for biomedical applications, these molecules have been tested as therapeutic agents in themselves. Some examples of G-quadruplex-based drugs are reported in the literature, such as antiviral oligonucleotides (23,24). Another example is the linear, four-stranded quadruplex $[d(T_2G_4T_2)]_4$, whose phosphorothioate backbone is considered to be responsible for strongly binding and inhibiting the gp120 envelope protein of the HIV (25). Finally, a 29mer 3′-modified phosphorodiester oligonucleotide (GRO29A) was reported by Bates *et al.* (26) as a potent growth inhibitor against several cancer cells *in vitro*. On the basis of these results, specifically modified GRO29A analogs were developed (27).

*To whom correspondence should be addressed. Tel: +33 1 40 79 36 89; Fax: +33 1 40 79 37 05; Email: mergny@vnumail.com
Present address:
Barbara Saccà, Laboratoire de Stabilité des Génomes, Institut Pasteur, 25 rue du Dr Roux, 75724 Paris cedex 15, France
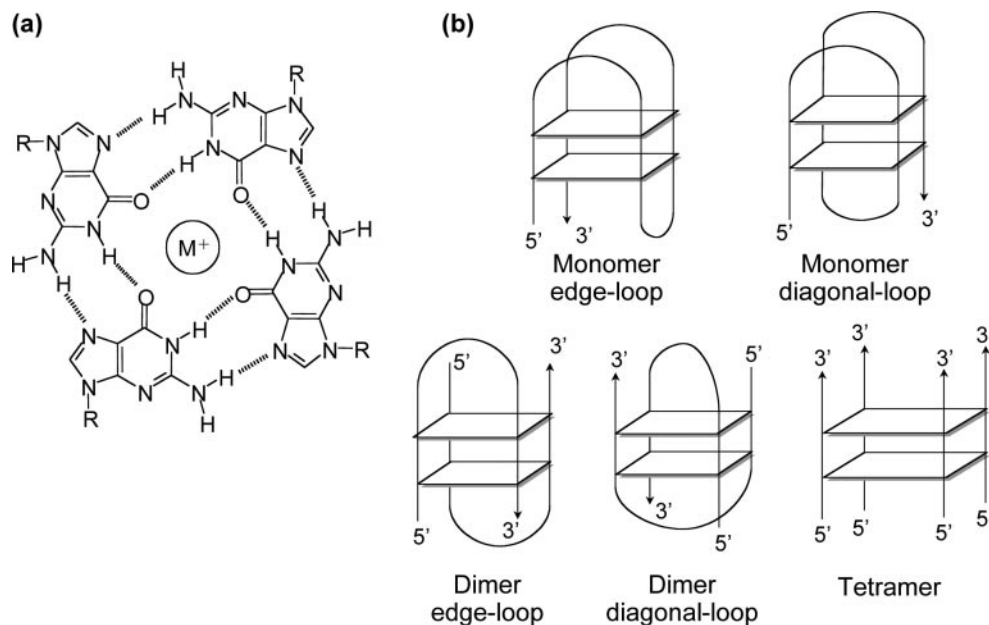
Figure 1. (**a**) Structure of a G-quartet: cyclic array of four guanines, linked by Hoogsten hydrogen bonds and stabilized by an internal positive ion. (**b**) Schematic representation of different G-quadruplex structures, with variable number and relative orientation of the self-associated strands and different orientation of the loops.

Thus, many progresses have been made on the elucidation of the biological roles of G-quadruplex structures (28). Nevertheless, new advancements are expected from a better understanding of the structural features of these unique DNA forms. To this purpose, NMR and X-ray crystallography studies can provide important information, even if the limitations due to their experimental condition requirements may give rise in some cases to contradictory results (29,30). On the other hand, biophysical methods, such as UV or CD spectroscopy (31) as well as calorimetry, can be easily applied under a variety of experimental conditions, allowing the determination of the influence of diverse parameters on the conformation and thermal stability of different G-quadruplex structures. Other studies have been reported on the thermodynamic and kinetic properties of G-quadruplexes (32), but only partial work has been carried out on the analysis of their chemically modified analogs.

In this paper, we report a systematic study of the thermal stabilities and thermodynamic properties of a variety of chemically modified G-quadruplexes. Their base sequences and names are listed in Table 1, while a schematic representation of the chemical modifications analyzed is given in Figure 2. The 15mer d($G_2T_2G_2TGTG_2T_2G_2$) oligonucleotide is known as the thrombin binding aptamer (15TBA) (33). Its 3D structure in potassium was elucidated by NMR and X-ray studies (34–36) and consists of two G-quartet planes connected by three lateral thymine loops (2TT and 1TGT) in a monomeric chair (or edge-loop) conformation. The 18mer oligonucleotide d($AG_2T_2AG_2T_2AG_2T_2AG_2$) contains the (TTAGG) motif of the *Bombyx mori* telomeric sequence which has also been found in other insects (37). The 22AG oligo contains four repeats of the human telomeric motif (TTAGGG) and has been observed to fold in sodium solution into an intramolecular G-quadruplex composed of three G-quartets connected by two lateral and one diagonal TTA loops (2,38). In potassium,

a different folding topology is observed (2,39). Finally, the bimolecular [d($G_4T_4G_4$)]$_2$ (12G4) and the tetramolecular [d(TG$_4$T)]$_4$ (TG4) oligonucleotides, both derived from the *Oxytricha nova* telomeric sequence, were also taken into consideration. The former forms a dimeric hairpin quadruplex in the presence of K$^+$, Na$^+$ or NH$_4^+$ cations in solution (40), while the latter forms a tetrameric quadruplex in the presence of sodium ions both in solution and in the crystalline state (41,42). Each unmodified oligonucleotide was compared with a series of synthetic analogs carrying either a backbone modification, such as the phosphorothioate (*S*) methylphosphonate (*M*) ribonucleotide (*R*) or 2′-*O*-methyl ribonucleotide (*O*) analogs. A schematic representation of the different synthetic analogs is given in Figure 2.

The purpose of this study is to examine the influence of a specific chemical modification on the thermal stability of different G-quadruplex structures in order to get a better insight into the factors regulating their formation and stabilization. The obtained information may be helpful for the development of new G-quadruplex-based therapeutic agents, as well as for a better exploitation of these structures in other fields, such as supramolecular chemistry and nanotechnologies (43).

MATERIALS AND METHODS

Oligonucleotides

All oligonucleotides were synthesized and purified by Eurogentec (Belgium). The primary sequences of the oligonucleotides are given in Table 1 and their nomenclature is explained in Figure 2. Analogs of the same series take the name of the corresponding regular unmodified DNA oligo and are distinguished by a suffix indicating the chemical modification. The -*S* and -*M* suffices, for example, refer to the phosphorothioate and methylphosphonate analogs.

Table 1. Names, sequences and melting temperatures (T_m or $T_{1/2}$) of G-quadruplex-forming oligonucleotides and their chemically modified analogs

Oligo series	Analog[a]	Sequence	$\varepsilon_{(260\ nm)}$[b] ($M^{-1}\ cm^{-1}$)	T_m ($T_{1/2}$)[c] (°C) NaCl	T_m ($T_{1/2}$)[c] (°C) KCl
15TBA	15TBA	d(**GGTTGGTGTGGTTGG**)	143300	≈20	48
	15TBA-*S*	d(**GGTTGGTGTGGTTGG**)	143300	≈20	43
	15TBA-*M*	d(**GGTTGGTGTGGTTGG**)	143300	–	–
	15TBA-*R*	r(**GGUUGGUGUGGUUGG**)	150500	n.r.	n.r.*
	15TBA-*O*	o(**GGUUGGUGUGGUUGG**)	150500	n.r. (≈10)	32
	15TBA-*U*	d(**GGUUGGUGUGGUUGG**)	150500	30	54
18TEL	18TEL	d(**AGGTTAGGTTAGGTTAGG**)	188100	40	42
	18TEL-*S*	d(**AGGTTAGGTTAGGTTAGG**)	188100	40	45
	18TEL-*M*	d(**AGGTTAGGTTAGGTTAGG**)	188100	–	–
	18TEL-*R*	r(**AGGUUAGGUUAGGUUAGG**)	196500	n.r. (≈25)	n.r.*
	18TEL-*O*	o(**AGGUUAGGUUAGGUUAGG**)	196500	≈14	22
	18TEL-*U*	d(**AGGUUAGGUUAGGUUAGG**)	196500	40	56
22AG	22AG	d(**AGGGTTAGGGTTAGGGTTAGGG**)	228500	55	62
	22AG-*S*	d(**AGGGTTAGGGTTAGGGTTAGGG**)	228500	57	63
	22AG-*M*	d(**AGGGTTAGGGTTAGGGTTAGGG**)	228500	33	43
	22AG-*R*	r(**AGGGUUAGGGUUAGGGUUAGGG**)	236900	48	n.r.*
	22AG-*O*	o(**AGGGUUAGGGUUAGGGUUAGGG**)	236900	44	66
	22AG-*U*	d(**AGGGUUAGGGUUAGGGUUAGGG**)	236900	54	62
12G4[d]	12G4	[d(**GGGGTTTTGGGG**)]$_2$	115200	*53*	*n.r.**
	12G4-*S*	[d(**GGGGTTTTGGGG**)]$_2$	115200	*44*	*n.r.**
	12G4-*M*	[d(**GGGGTTTTGGGG**)]$_2$	115200	–	–
	12G4-*R*	[r(**GGGGUUUUGGGG**)]$_2$	121000	*40*	*n.r.**
	12G4-*O*	[o(**GGGGUUUUGGGG**)]$_2$	121000	*41*	*n.r.**
	12G4-*U*	[d(**GGGGUUUUGGGG**)]$_2$	121000	*50*	*n.r.**
TG4[e]	TG4	[d(**TGGGGT**)]$_4$	57800	*55*	*>90*
	TG4-*S*	[d(**TGGGGT**)]$_4$	57800	*48*	*>90*
	TG4-*M*	[d(**TGGGGT**)]$_4$	57800	–	*>90*
	UG4-*R*	[r(**UGGGGU**)]$_4$	60000	*>80*	*>90*
	UG4-*O*	[o(**UGGGGU**)]$_4$	60000	*75*	*>90*
	UG4-*U*	[d(**UGGGGU**)]$_4$	60000	*65*	*>90*

The oligos were prepared at 5 or 10 μM strand concentration in 10 mM sodium cacodylate buffer at pH 7.0 containing 100 mM NaCl or 100 mM KCl.
[a]For each series of oligonucleotides, the thermal stabilities of the unmodified oligos (i.e. 15TBA, 18TEL, 22AG, 12G4 and TG4) were compared with the ones of their synthetically modified analogs. These are indicated as follows: *S*, phosphorothioate; *M*, methylphosphonate; *R*, ribonucleotide (T→U and 2′-H→2′-OH); *U*, deoxyribonucleotide (T→U and 2′-H) and *O*, 2′-*O*-methyl-ribonucleotide (T→U and 2′-H→2′-*O*-Me).
[b]The extinction coefficients (ε) for the oligos were calculated as described in Materials and Methods.
[c]T_ms values for the reversible transitions of the intramolecular compounds or apparent melting temperatures ($T_{1/2}$) indicated in italics, for the non-reversible processes of the bi- and tetramolecular complexes. The process is indicated as '–' for no transition (the T_ms is too low to be detected with accuracy); n.r., for non-reversible transition; and n.r.*, for non-reversible multi-phase transition either in the cooling or in the heating profile.
[d]For the 12G4 series, the transitions are not reversible in the experimental conditions and show different degrees of hysteresis. Averaged values of $T_{1/2}$ (between the cooling and heating process) are given for the oligos in sodium buffer. Their values depend from the scan rate and are provided for a 0.2°C per minute temperature gradient.
[e]In the experimental conditions, the thermal transitions of the TG4 series are irreversible. $T_{1/2}$ values that depend on the temperature gradient chosen for the experiment reflect the temperature dependency of the dissociation process (45). Only the initial melting processes could be observed in sodium buffer and their apparent melting temperatures, $T_{1/2}$, are provided for a 0.2°C per minute temperature scan rate.
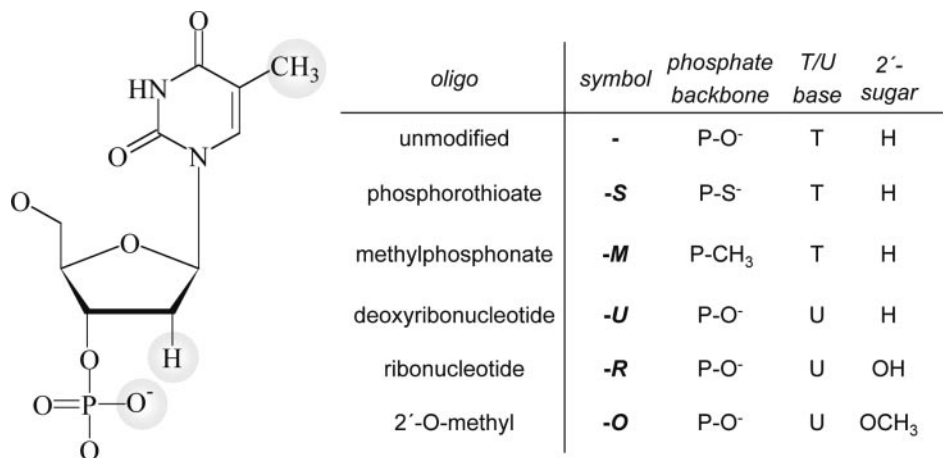

Figure 2. Schematic representation of the chemical modifications examined in this work and nomenclature used to designate the different modified oligonucleotides. The backbone modified oligos are indicated as oligo-*S* for the phosphorothioate analogs and oligo-*M* for the methylphosphonate analogs. The deoxyribonucleotide derivatives (T→U substitution only) are indicated as oligo-*U*. Additional modification at the sugar level is indicated as oligo-*R* for the ribonucleotide analogs or oligo-*O* for the 2′-*O*-methyl-ribonucleotide analogs.

The deoxyribonucleotide analogs containing a T→U substitution are indicated by an -*U* suffix, whereas the ribonucleotide and the 2′-*O*-methyl ribonucleotide analogs are indicated by an -*R* and an -*O* suffix, respectively. The concentrations of the oligonucleotides, expressed in single-strand molarity, were determined by UV absorption at 260 nm using a 'nearest-neighbor' approximation (44).

UV-thermal curves

Unless stated differently, all experiments were performed in a 10 mM sodium cacodylate buffer at pH 7.0 containing 100 mM NaCl (in the text it will be shortly referred to as sodium buffer) or 100 mM KCl (potassium buffer). The intramolecular and bimolecular G-quadruplex-forming oligonucleotides were typically prepared at 5 and 10 µM strand concentration, respectively. Concentration dependency of the melting temperatures was tested in the 0.5–50 µM range (for 22AG), 1–50 µM (for 15TBA; see Supplementary Figure S1a), 1–20 µM (for 22AG-*O*, *S*, *R*; see Supplementary Figure S1b and S1c), 5–500 µM (for TG4), 10–200 µM (for TG4-*O* and TG4-*R*), 10–40 µM (for TG4-*U* and TG4-*S*) or 3–15 µM (for other sequences). After denaturation at 95°C, the solutions were slowly cooled at room temperature and finally allowed to equilibrate at 4°C overnight. Tetramolecular G-quadruplexes, instead, were pre-formed for 1 week at 4°C at 200–300 µM strand concentration in 1 mM sodium cacodylate buffer in the presence of 100 mM NaCl or KCl. The tetramolecular complexes were then diluted to 10 µM strand concentration in sodium or potassium buffer. This long equilibration time at a relatively high strand concentration has been chosen because of the extreme kinetic inertia of these tetramolecular complexes (45). Thermal denaturation and renaturation curves were obtained with a Kontron Uvikon 940 spectrophotometer using quartz optical cells of 0.2–1 cm pathlength (46). The intramolecular and bimolecular G-quadruplex solutions were heated at 92°C for 10 min and the folding/unfolding processes were recorded in the 92 to −2°C temperature range (and vice versa), using a scan rate of 0.2°C min^{-1} and following the variation of UV absorption at 295 nm (47).

UV-thermal difference spectra

For each oligonucleotide sample, an UV spectrum was recorded above and below its melting temperature (T_m). The difference between the UV spectrum at high temperature (82°C) and the UV spectrum at low temperature (8°C) is defined as the thermal difference spectrum and represents the spectral difference between the unfolded and the folded form. Differential spectra have a typical and unique shape for quadruplexes and can be used as a simple and rapid method to identifying these structures and to get further information on their 3D organization (47,48). The thermal difference spectra are normalized, giving a value of +1 for the highest positive peak.

UV thermodynamic analysis

Analysis of the thermal curves was performed with Kaleida-Graph 3.5 software. Van't Hoff thermodynamic analysis was carried out only for the intramolecular G-quadruplex oligonucleotides. In fact, their thermal reversibility (superimposable heating and cooling profiles) allowed the calculation of the value of the equilibrium constant (K) assuming a simple two-state model. Application of the Van't Hoff equation ($\ln K = -\Delta H_{VH}/RT + \Delta S_{VH}/R$) yielded to the determination of the enthalpy (ΔH_{VH}) and entropy (ΔS_{VH}) of the process, as described elsewhere (46). Nevertheless, the Van't Hoff analysis could not be performed for the 22AG-*O* and 22AG-*U* analogs as the plot of $\ln K$ versus $1/T$ appeared to be more complicated.

Differential scanning calorimetry

Microcalorimetry experiments were performed on the 22AG series using a Nano DSC-II microcalorimeter (CSC) driven by a DSC-run software. The oligonucleotides were dissolved at a concentration ranging from 50 to 70 µM in 10 mM sodium cacodylate buffer at pH 7.2 containing 100 mM KCl. Solutions were carefully degassed prior to their utilization and their thermal profiles were analyzed in the 0–95°C temperature range at a scan rate of 1°C per minute. An initial calibration of the instrument was performed by filling both the reference and the sample cells with the buffer solution and accumulating several scans till the balance was reached. A baseline-corrected DSC curve of the sample was obtained by loading the solution of oligonucleotide into the sample cell and performing the thermal scans in the same experimental conditions as for the baseline determination. A minimum of six scans was collected for each experiment to check out the reversibility of the thermal process. Normalization of the DSC curve and calculation of the thermodynamic parameters were carried out using the Cp-calc software (Applied Thermodynamics), where the heat capacity variation of the baseline from the pre- to the post-transition line was best represented by a linear-polynomial function. The calorimetric enthalpy (ΔH_{cal}) and entropy (ΔS_{cal}) for the transition process was determined directly from the DSC curve, i.e. in a model-independent way. Comparison of the ΔH_{cal} with the Van't Hoff value obtained by the UV-thermal curve (ΔH_{VH}) allowed the verification of the correctness of the previously assumed two-state model to describe the entire thermal process ($n = \Delta H_{VH}/\Delta H_{cal} = 1$).

RESULTS

The equilibrium T_ms of the oligonucleotides or the temperatures of half transition ($T_{1/2}$: for non-superimposable heating and cooling profiles), both in Na$^+$ and K$^+$ buffer, are listed in Table 1.

15 and 18mers

As shown in Figure 3a and Supplementary Figure S2 for the 15TBA series in K$^+$ and Na$^+$ buffer, respectively, the oligonucleotides gave quite different melting profiles depending on the particular chemical modification. The methylphosphonate oligo (15TBA-*M*) gave no observable transition, resulting in a flat thermal profile. In contrast, the unmodified 15TBA oligo gave a reversible transition with a T_m of 48°C in K$^+$. The 15TBA-*O*, the 15TBA-*S* and the 15TBA-*U* analogs, instead, showed reversible transitions, with concentration-independent T_ms of 32, 43 and 54°C, respectively (see Table 1). Interestingly, the RNA analog (15TBA-*R*) presented a complex behavior with a non-superimposable and multiphasic response upon heating and cooling (hysteresis, see Figure 3 and Supplementary Figure S2, squares).
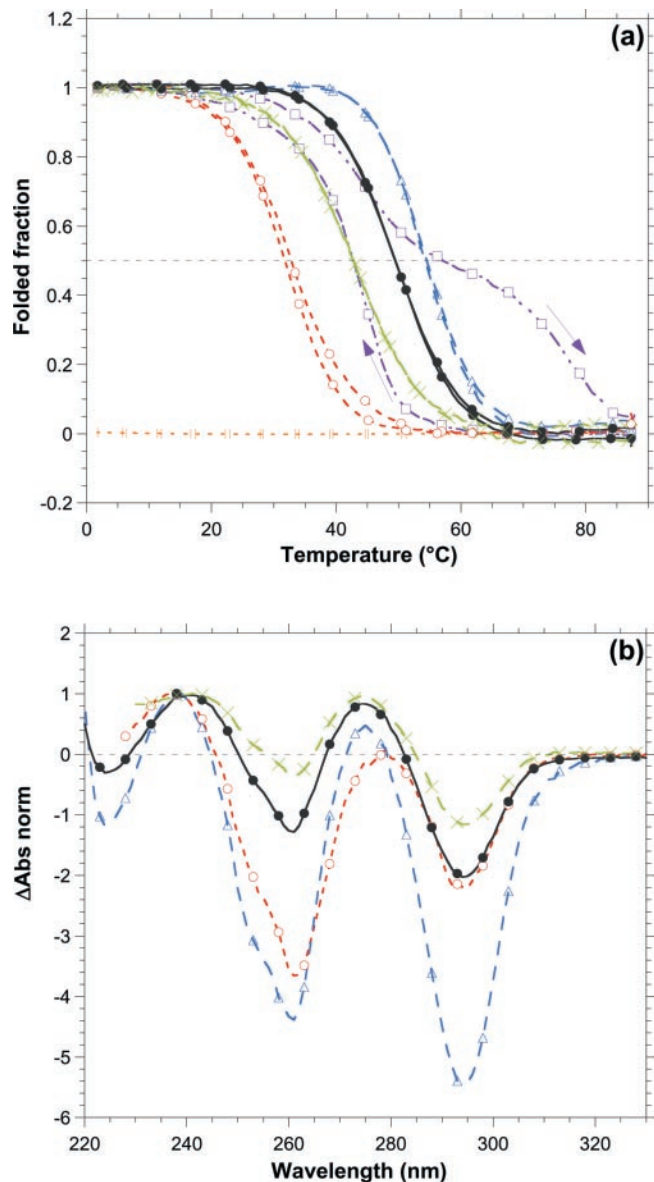
Figure 3. (**a**) Normalized thermal transition profiles measured at 295 nm and (**b**) normalized differential spectra in the 220–340 nm region for the 15TBA oligo and its analogs at 5 μM (or 3 μM for 15TBA-*S*) strand concentration in 10 mM sodium cacodylate buffer pH 7.0 containing 100 mM KCl. 15TBA (black full circles), 15TBA-*S* (green crosses), 15TBA-*M* (yellow vertical bars), 15TBA-*R* (violet open squares), 15TBA-*O* (red open circles) and 15TBA-*U* (blue open triangles). An hysteresis phenomenon occurs for the 15TBA-*R* and the direction of the temperature gradient is indicated by the arrows.

The normalized differential spectra for the 15TBA and its *S*-, *U*- and *O*-analogs in K$^+$ buffer are shown in Figure 3b. The spectra exhibit the typical pattern of an intramolecular G-quadruplex structure (47,48), with two positive maxima at 240 and 275 nm and two negative minima at ∼260 and 295 nm. Interestingly, the differential spectra of the unmodified oligo and its *S*- and *U*-derivatives are similar in shape. In contrast, the differential spectrum of the 15TBA-*O* analog shows a peculiar shape with a ratio between the two negative minima which is inverted in comparison with the one obtained for the other three species.

Analogous results were obtained for the 18TEL oligonucleotide series in the same buffer conditions (Supplementary Figure S3a and S3b for Na$^+$ and K$^+$): no transition was observed for the backbone-modified oligo 18TEL-*M*, whereas reversible transitions were detected for the unmodified oligo as well as for the *O*-, *S*- and *U*-derivatives. Similarly, a non-reversible transition was observed for the RNA analog (18TEL-*R*). Moreover, as reported in Table 1, the 15TBA and 18TEL series in K$^+$ buffer presented the same order of thermal stability for the different modified oligos, being:

15TBA-*M* ≪ 15TBA-*O* < 15TBA-*S* < 15TBA < 15TBA-*U*

and

18TEL-*M* ≪ 18TEL-*O* < 18TEL ≈ 18TEL-*S* < 18TEL-*U*.

Interestingly, the differences between the T_ms of the various species are more pronounced in the 18TEL series (max $\Delta T_m = 34°C$) than in the 15TBA series (max $\Delta T_m = 22°C$). Analysis of the 15TBA and 18TEL oligo series in Na$^+$ buffer (Supplementary Figures S2 and S3a) gave lower values of T_m and reduced variations between the modified analogs of the same series (see Table 1). It is also worth mentioning that for DNA, RNA, phosphorothioates, 2′-*O*-methyl and dU-containing oligomers, the differences between Na$^+$ and K$^+$ are relatively modest in the 18TEL series (maximum difference 8°C; compare the two rightmost columns in Table 1), but very important in the TBA series (T_m is 20–28°C higher in K$^+$). In other words, although K$^+$ is preferred over Na$^+$ for all quadruplexes, this preference is much more pronounced for 15TBA and its analogs.

Finally, a detailed thermodynamic analysis of the unmodified oligo and its *S*-, *O*- and *U*-derivatives was performed for both the 15TBA and 18TEL series in potassium buffer. We initially checked the concentration independency of the T_m of these analogs (see Supplementary Figure S1a for 15TBA in the 1–50 μM strand concentration range). The UV-thermal transition curves were analyzed using the Van't Hoff equation and assuming a two-state model (all-or-none) to describe the single-strand to quadruplex process. The results obtained are reported in Table 2. The highest values (in absolute terms) of ΔH_{VH} and ΔS_{VH} were found in the case of the *U*-species and resulted in the most negative values of ΔG_{VH} at 37°C (-2.52 kcal mol^{-1} for the 15TBA-*U* and -2.81 kcal mol^{-1} for the 18TEL-*U*). In contrast, the *O*-derivatives presented the least favorable values of ΔG_{VH} (+0.60 kcal mol^{-1} for the 15TBA-*O* and +1.46 kcal mol^{-1} for the 18TEL-*O*), resulting in the least stable structures at 37°C. Remarkably, the differences between the four analogs are more evident in the 18TEL series as compared with the 15TBA series.

Human telomeric motif (22AG)

For the 22AG series, the UV-thermal transition curves were measured both in Na$^+$ and K$^+$ buffer (Supplementary Figure S4a and S4b, respectively) and the values of their T_ms are reported in Table 1. In both buffer conditions, the 22AG-*M* oligonucleotide appeared to be less stable than the other modified analogs. In contrast, both 22AG-*S* and 22AG-*U* gave reversible curves with T_ms similar to the one of their corresponding unmodified forms. T_m values were concentration-independent for all oligomers (examples shown

Table 2. Van't Hoff thermodynamic parameters for the reversible thermal renaturation of the 15TBA and 18TEL oligonucleotides and their *O*-, *U*- and *S*-analogs

Oligonucleotide	T_m (°C)	ΔH_{VH} (kcal mol^{-1})	ΔS_{VH} (kcal mol^{-1} K^{-1})	ΔG_{VH} (37°C) (kcal mol^{-1})
15TBA	48	−39.7	−0.123	−1.57
15TBA-*O*	32	−39.7	−0.130	+0.60
15TBA-*U*	54	−48.4	−0.148	−2.52
15TBA-*S*	43	−35.2	−0.112	−0.48
18TEL	42	−37.9	−0.120	−0.70
18TEL-*O*	22	−34.5	−0.116	+1.46
18TEL-*U*	56	−49.0	−0.149	−2.81
18TEL-*S*	45	−38.3	−0.120	−1.10

The oligos were prepared at 5 µM strand concentration in 10 mM sodium cacodylate buffer at pH 7.0 containing 100 mM KCl. Van't Hoff enthalpy and entropy changes (ΔH_{VH} and ΔS_{VH}) for the reversible thermal transitions were calculated according to the equation $\ln K(T) = -\Delta H_{VH}/RT + \Delta S_{VH}/R$, where K is the equilibrium constant for the G-quadruplex transition and was determined by the UV-thermal curve. Plotting of $\ln K(T)$ versus $1/T$ allowed to obtain the values of ΔH_{VH} and ΔS_{VH}, respectively, from the slope and the intercept of the linear regression. Free energies (ΔG_{VH}) were calculated at 37°C using the Gibbs equation $\Delta G_{VH}(T) = \Delta H_{VH} - T\Delta S_{VH}$.

in Supplementary Figure S1b and S1c). Additionally, all T_m values in sodium buffer were 7–22°C lower than in potassium buffer. Of particular interest is the behavior of the RNA and 2′-*O*-methyl analogs (22AG-*R* and 22AG-*O*), which gave a relatively low T_m in Na$^+$ buffer (48 and 44°C), but in K$^+$ represented the most stable forms with a multiphasic thermal profile, respectively in the case of RNA (Supplementary Figure S4a and S4b).

The conformational properties of the reversible 22AG oligos, i.e. the 22AG, 22AG-*S*, 22AG-*O* and 22AG-*U*, were analyzed by differential absorbance spectra as illustrated in Figure 4. In sodium buffer (Figure 4a), the differential spectra for all the species showed two positive maxima at ∼245 and 270 nm, a shoulder at 255 nm and a negative minimum at 295 nm. However, while the differential spectra of the 22AG and its *S*- and *U*-derivative were almost superimposable, the profile of the 22AG-*O* was slightly different owing to the higher value of ΔAbs at 245 nm. Similarly, as illustrated in Figure 4b, the differential spectra of the 22AG and its *S*- and *U*-analog in potassium buffer were almost identical. However, while their maximum and minimum peaks were positioned at the same wavelength values as in sodium buffer, the ratio between their intensities was different in the two buffer conditions. On the other hand, the differential spectrum of the 22AG-*O* in potassium buffer appeared to be quite unrelated to all the others, though its anomalous shape reminded the one of the 15TBA-*O* in the same buffer conditions (cf. Figures 4b and 3b).

Finally, DSC experiments were performed on the 22AG and its *O*- and *U*-derivatives in potassium buffer and their calorimetric values of enthalpy (ΔH_{cal}) and entropy (ΔS_{cal}) of renaturation are reported in Table 3. In the case of the 22AG, the Van't Hoff enthalpy determined by the analysis of the UV-thermal transition curve ($\Delta H_{VH} = -45.0$ kcal mol^{-1}) was compared with the calorimetric value obtained by DSC ($\Delta H_{cal} = -41.5$ kcal mol^{-1}), giving a ratio $n = \Delta H_{VH}/\Delta H_{cal}$ of ∼1 ($n = 1.08$). The similarity of the two values validated the hypothesis of the two-state model used in the Van't Hoff analysis to describe the thermal transition of the
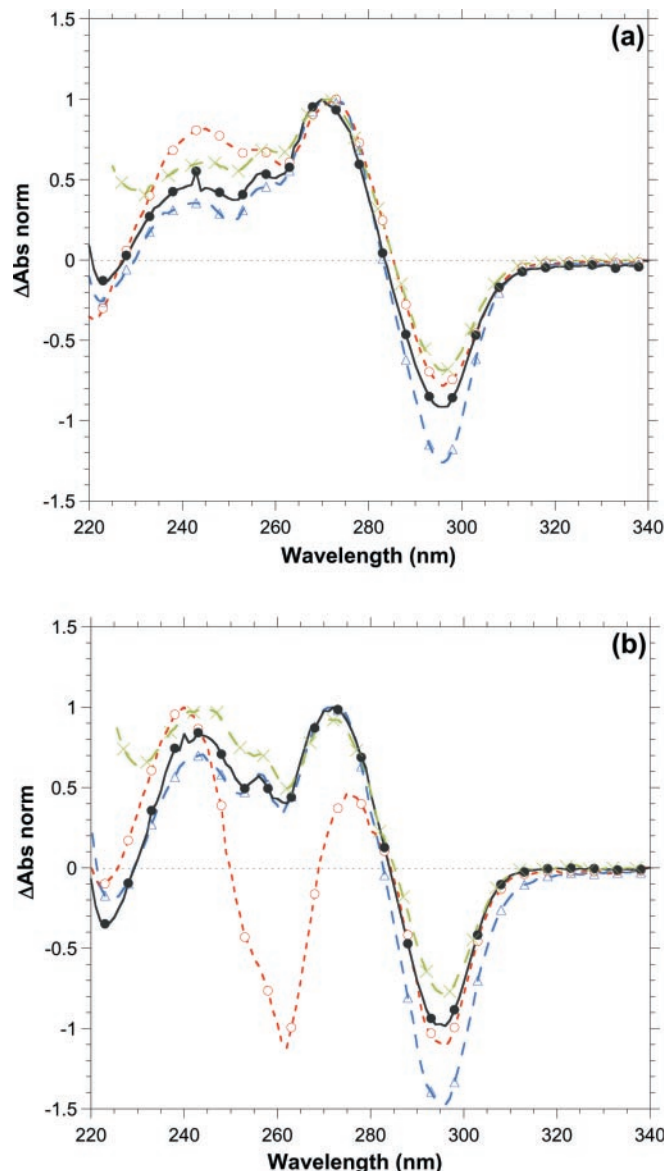
Figure 4. Normalized differential spectra in the 220–340 nm region for the 22AG oligo and its *S*-, *O*- and *U*-analogs at 5 µM strand concentration in 10 mM sodium cacodylate buffer pH 7.0 containing (**a**) 100 mM NaCl or (**b**) 100 mM KCl. 22AG (black full circles), 22AG-*S* (green crosses), 22AG-*O* (red open circles) and 22AG-*U* (blue open triangles).

Table 3. Calorimetric values of enthalpy and entropy of renaturation for the 22AG oligo and its *O*- and *U*-derivatives

Oligo	T_m^{cal} (°C)	ΔH_{cal} (kcal mol^{-1})	ΔS_{cal} (kcal mol^{-1} K^{-1})
22AG	64	−41.5[a]	−0.123
22AG-*O*	66	−23.5	−0.069
22AG-*U*	63	−33.2	−0.097

For the DSC experiments, the oligos were prepared at ∼50–70 µM strand concentration in 10 mM sodium cacodylate buffer at pH 7.0 containing 100 mM KCl. Calorimetric values of ΔH_{cal} and ΔS_{cal} for the reversible thermal transitions were obtained by the DSC profiles (variation of heat capacity versus temperature), using the Cp-Calc software.
[a]Comparison between the ΔH_{VH} (−45.0 kcal mol^{-1}) and the ΔH_{cal} (−41.5 kcal mol^{-1}) for the thermal renaturation of the 22AG oligo gave a ratio n of ∼1 ($n = 1.08$). This confirmed the monomolecularity of the process and the validity of the two-state transition model assumed in the Van't Hoff analysis.

intramolecular G-quadruplex. However, in the case of the 22AG-*O* and 22AG-*U*, the plot of ln$K$ versus 1/T appeared quite complex (presence of a pre-transition visible on supplementary Figure S4b) and could not be described by a simple Van't Hoff equation. For this reason, only the calorimetric (model independent) thermodynamic parameters were determined and their values are reported in Table 3. Comparison between the ΔH_{cal} values of the three species allows us to establish the following order of renaturation enthalpy (in absolute terms): 22AG-*O* < 22AG-*U* < 22AG. The same tendency was observed for the ΔS_{cal}, thus counteracting the contribution given by the ΔH_{cal} and yielding to similar T_ms for the three species [max $\Delta T_m s^{(cal)} = 3°C$]. The following order of thermal stability in potassium can be therefore established for the 22AG series:

$$22AG\text{-}M \ll 22AG \approx 22AG\text{-}S \approx 22AG\text{-}U \approx 22AG\text{-}O.$$

Bimolecular (12G4) and tetramolecular (TG4) quadruplexes

The stabilization of the bimolecular and tetramolecular G-quadruplex-forming oligonucleotides in potassium buffer did not allow us to record the half-point of the thermal transitions in the temperature range analyzed (see Table 1). In sodium buffer, instead, the apparent melting temperatures ($T_{1/2}$) for both the 12G4 and TG4 oligo series could be determined and their values are reported in Table 1. As illustrated also in Figure 5a and c, the methylphosphonate analogs (12G4-*M* and TG4-*M*) gave no observable transitions, as for 15TBA-*M* and 18TEL-*M*. However, the shape of the thermal profiles for all the other oligonucleotides were affected by the kinetics of the process (heating/cooling scan rate), resulting in hysteresis curves in the 12G4 series ($T_{1/2}$ values for the cooling and heating process were different) and in irreversible transitions in the TG4 series ($T_{1/2}$ values were determined only for the heating process).

In the bimolecular series, the unmodified oligo and its *U*-derivative were the most stable forms in Na$^+$ (as judged from the $T_{1/2}$ values for the cooling and heating processes), presenting similar T_ms and a larger hysteresis effect in comparison with the other bimolecular G-quadruplexes (see Figure 5a). Therefore, the following order of increasing $T_{1/2}$ can be established for the 12G4 series in sodium buffer:

$$12G4\text{-}M \ll 12G4\text{-}R \approx 12G4\text{-}O \approx 12G4\text{-}S < 12G4\text{-}U \approx 12G4$$

The relatively large hysteresis found for some samples of the 12G4 series allowed a kinetic analysis, in a manner similar to triplexes or *i*-tetraplexes. The hysteresis found for 12G4-*O* is minimal (Supplementary Figure S5G) and intermediate for the phosphorothioate sample (Supplementary Figure S5C). Arrhenius plots for 12G4, 12G4-*S*, *R*, *O* and -*U* are shown in Supplementary Figure S5B-J. As observed for tetramolecular quadruplexes (45), a negative apparent activation energy of association is found for 12G4 and the -*S*, -*U* analogs (i.e. folding is faster at low temperature, $E_{on} = -34$ to -42 kcal mol^{-1}), demonstrating that the association process does not correspond to an elementary step. Concerning dissociation, a non-linear relationship is found for 12G4 and 12G4-*U*; it is, therefore, difficult to interpret the k_{off} data and thus provide

E_{off} and ΔH_{VH}^0 values, as no satisfactory fit may be proposed for the dissociation process (Supplementary Figure S5B and S5J). Overall, between the different analogs (with the exception of the RNA sample), the differences in k_{on} (and E_{on}) were less pronounced than the differences in k_{off}.

The differential spectra of the unmodified 12G4 and its *S*- and *U*-analog in sodium buffer are illustrated in Figure 5b. The three species gave almost superimposable ΔAbs curves, with two positive maxima at 245 and 275 nm, a shoulder at ∼255 nm and a negative minimum at 295 nm. It is worth noting the similarity of these differential spectra with the ones of the 22AG and its *S*- and *U*-derivatives in the same buffer conditions (cf. Figures 5b and 4a). Moreover, in the same way as for the intramolecular 22AG-*O*, also the bimolecular *O*-derivative (12G4-*O*) presented an unusual shape of its differential spectrum in Na$^+$, with a larger value of relative intensity at 245 nm.

Quite different was, instead, the order of $T_{1/2}$ for the tetramolecular complexes in sodium buffer, as it can be seen from Figure 5c, being:

$$TG4\text{-}M \ll TG4\text{-}S < TG4 < TG4\text{-}U < TG4\text{-}O \ll TG4\text{-}R.$$

In particular, the thermal denaturation of the ribonucleotide analog (TG4-*R*) was still not complete even at 85°C (45) and could not be taken into consideration in the analysis of the differential spectra. These melting profiles actually solely reflect the dissociation of the quadruplexes, explaining why these $T_{1/2}$ values appear concentration-independent (45).

The differential spectra of the unmodified TG4 oligonucleotide and its *S*-, *O*- and *U*-derivatives in sodium buffer are reported in Figure 5d. Once again, the maximum and minimum peaks were found to be centered at the same wavelength values as for the differential spectra of the 12G4 and 22AG quadruplexes, i.e. at 245, 275 and 295 nm, with a shoulder at 255 nm. Interestingly, the shape of the differential spectrum of the TG4 oligo in sodium buffer is quite similar to the one obtained for the 22AG oligo in potassium buffer (cf. Figures 5d and 4b). Additionally, one can notice a certain similarity in the ΔAbs profile of the unmodified G-quadruplex (TG4) and its *S*- and *U*-analogs, with a ratio between their intensities at 245 and 275 nm, which is increasing almost in the same way as their thermal stabilities. Finally, as previously remarked for the bimolecular and the 22AG series, the tetramolecular *O*-derivative showed a peculiar differential spectrum as compared with the ones of the same oligo series: the shoulder at 255 nm disappeared and the ratio between the intensities at 245 and 275 nm reached the highest value.

DISCUSSION

With the growing evidence of the importance of G-quadruplex structures *in vivo*, a comprehensive knowledge of the structural properties of these oligonucleotides appears more and more essential. Several biophysical studies have been realized in the past 10 years on different G-quadruplex structures (1), yielding to a wide amount of thermodynamic and kinetic data summarized in a recent review (32). The wide polymorphism observed in G-quadruplex structures has to be attributed to a subtle balance of different factors. Of primary importance are
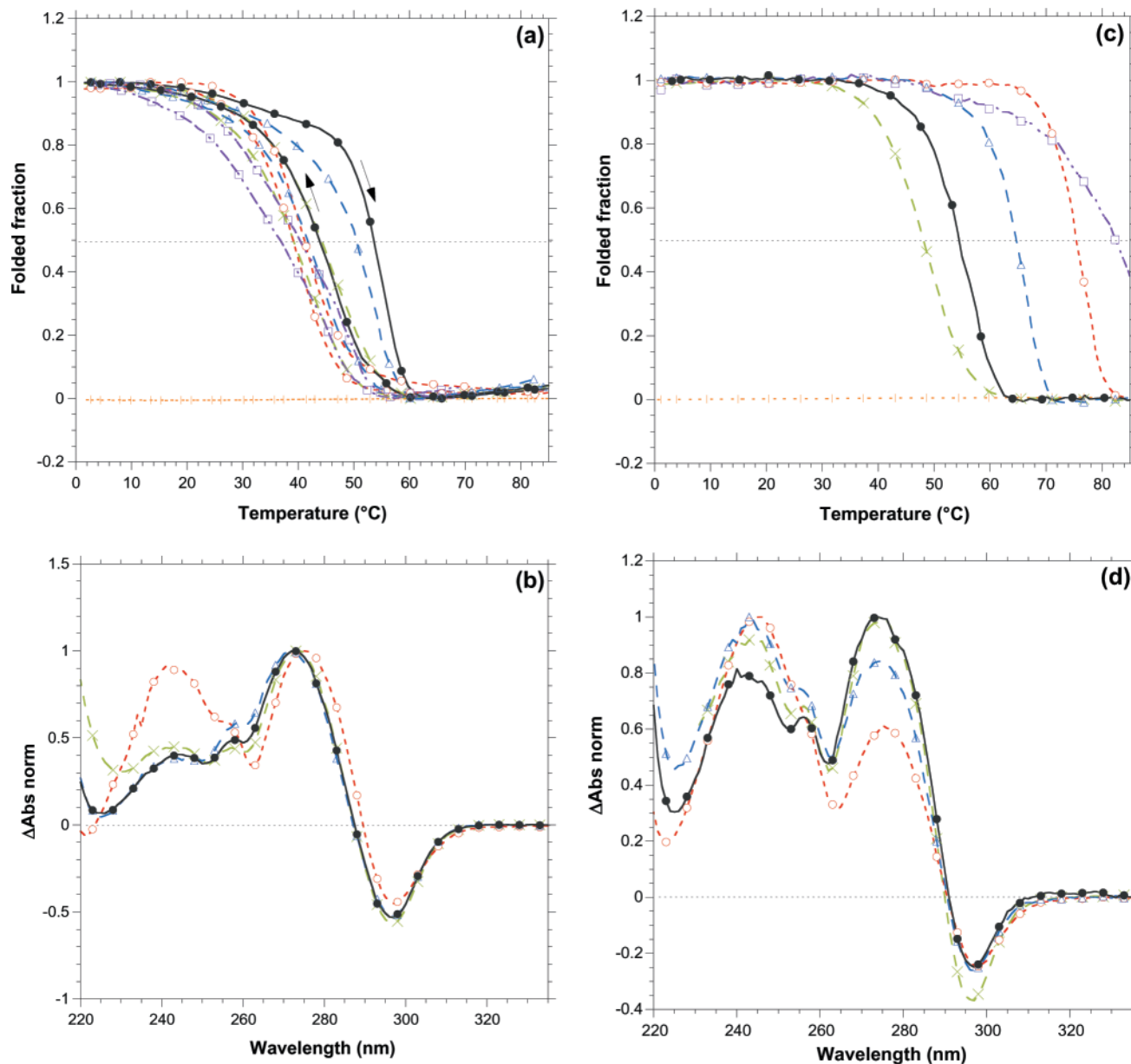
Figure 5. Normalized thermal denaturation profiles measured at 295 nm and normalized differential spectra in the 220–340 nm region for the 12G4 series [(**a**) and (**b**), respectively] and TG4 series [(**c**) and (**d**), respectively] at 10 µM strand concentration in 10 mM sodium cacodylate buffer, pH 7.0, containing 100 mM NaCl. 12G4 and TG4, black full circles; 12G4-*S* and TG4-*S*, green crosses; 12G4-*M* and TG4-*M*, yellow vertical bars; 12G4-*R* and TG4-*R*, violet open squares; 12G4-*O* and TG4-*O*, red open circles; and 12G4-*U* and TG4-*U*, blue open triangles. Upon cooling, no renaturation of the TG4 quadruplexes is obtained, and further heating/cooling cycles led to a similar monotonous variation of absorbance with no evidence for quadruplex reformation or denaturation.

DNA sequence and strand concentration, as well as the presence of monovalent cations, such as Na+ and K+, but a large set of secondary forces, such as base-stacking interactions, hydrogen bonding and hydrophobic effects may significantly contribute to the stabilization of the final structure. As described in this paper, the effect of different factors on the modulation of G-quadruplex conformation was evaluated using modified G-quadruplex-forming oligonucleotides.

Methylphosphonate analogs

For all the G-quadruplexes analyzed, loss of the negative charge at the level of the phosphate backbone, as in the methylphosphonate analogs, leads to a strong destabilization of the G-quadruplex structure, independently from its molecularity (see Table 1). This result is in agreement with the evidences accumulated by several crystal structures (42,49,50), in which the negatively charged oxygen atoms of the backbone were found to be involved in a complex pattern of water-bridges with the sugar groups and the edges of the guanine units. These extensive hydrogen-bonding interactions give rise to a well-ordered distribution of water molecules along the G-quadruplex grooves, also called hydration spines, which seem to be relevant for the stabilization of the structure. However, this does not necessarily imply that non-negatively charged oligomers cannot

form G-quadruplexes, as recently demonstrated by the formation of a DNA_2–PNA_2 (peptide nucleic acid) hybrid quadruplex or PNA_4 quadruplex (51,52).

Phosphorothioate analogs

Not only the charge but also the ionic radius of the atom of the oligonucleotide backbone may have an impact in the formation and stabilization of G-quadruplex structures. Substitution of the oxygen atoms of the phosphate backbone with sulfur atoms appears to affect the stability of the G-quadruplex structure in a molecularity-dependent way. In fact, in the bimolecular and tetramolecular phosphorothioate oligos (12G4-*S* and TG4-*S*), the larger size of the S^- in comparison with the O^- destabilizes the G-quadruplex. However, the different spatial arrangement of the intramolecular complexes seems to be less affected by the presence of sulfur ions, leading to quasi equivalent T_ms with respect to the one of the unmodified species (see Table 1, 15TBA, 18TEL and 22AG).

2′-sugar modified analogs

Interesting observations emerge from the comparative analysis of the unmodified oligos and their *O*- and *U*-analogs in the different G-quadruplex forms. In both the 15TBA and 18TEL series, the order of thermal stability is *O*-analog < unmodified ≤ *U*-analog. This suggests a stabilizing role of the T→U base substitution, which is, however, counteracted by a stronger destabilizing effect of the 2′-sugar modification. These results may have notable implications for a better understanding of the role of thymine loops in the stabilization of intramolecular G-quadruplex structures, though more remarkable appears the role of the 2′-position of the sugar moiety. In fact, substitution of the ribose 2′-H with a methoxy group (*O*-analog) can yield not only to a destabilization of the structure, as observed for the 15TBA and 18TEL series, but also to a complete changing of the quadruplex conformation, as shown by the differential spectrum of the 15TBA-*O* in potassium buffer (Figure 3b). On the other hand, substitution of the 2′-H of the sugar moiety with an hydroxy group (*R*-analog) may result in thermal hysteresis, as in the case of the 15TBA-*R* and 18TEL-*R* oligos both in sodium and potassium buffer (Table 1, Figure 3a and Supplementary Figures S2 and S3). This 'atypical' thermal inertia for the intramolecular ribonucleotide analogs may be possibly originated by a change of sugar conformation into a 'more rigid' form. However, structural studies are required to better understand this event.

In addition, the same 2′-sugar modifications seem to have different structural effects depending on the molecularity of the G-quadruplex. A 2′-methoxy substitution yields to a destabilization of the structure in the short intramolecular G-quadruplexes (15TBA and 18TEL series), resulting in the following order of thermal stability: *O*-analog < unmodified ≤ *U*-analog. However, the same modification in the tetramolecular complexes (TG4 oligos) leads to a strong stabilization of the structure. Likewise, the ribonucleotide analogs (2′-OH substitution) show quite different thermal stabilities in the intra- and tetramolecular compounds, giving rise to intermediated values of $T_{1/2}$ in the former (15TBA-*R* and 18TEL-*R*, with hysteresis) and to incomplete denaturation in the latter (TG4-*R*). RNA, DNA and 2′-*O*-methyl tetramolecular

G-quadruplexes exhibit a fourth order dependence of the association rate, a negative energy of activation for association and a strongly positive energy of activation for dissociation (45). The extreme stability of parallel RNA tetramolecular quadruplexes as compared with DNA quadruplexes results both from a much faster association and a slower dissociation. This difference might be explained by the greater difficulty in adopting a *syn* conformation for the ribonucleoside residues (53), making the formation of parallel quadruplexes favorable as compared with antiparallel quadruplexes. Interestingly, a similar sugar-dependent stabilization effect has been recently found for locked nucleic acid (LNA) oligomers (54). LNAs may form parallel tetramolecular G-quadruplexes, whose 'locked' sugar conformation leads to a thermal stability comparable with that of TG4-*R* (54). In the bimolecular (12G4) series, and even more in the human telomeric sequence (22AG) series, modification of the ribose 2′-position does not strongly affect the thermal stability of the G-quadruplex structure (see Figure 5a, Supplementary Figure S4 and Table 1). However, it is worth noting that in all series of G-quadruplexes in K^+, independently on their molecularity, substitution of the 2′-H of the ribose ring with a 2′-*O*-methyl (*O*-analogs) definitely leads to a change in the quadruplex conformation, as it is evidenced by all the differential spectra of the *O*-species reported in this work.

From these findings, one can presume the participation of the 2′-position of the sugar moiety in crucial interactions, which may be modulated by the possibility to form hydrogen bonds. However, other molecularity-dependent structural features seem to be involved in the stabilization of G-quadruplexes and additional studies would be necessary to investigate the role of this new factor.

Human telomeric sequence (22AG)

Different from all the other oligo series, thymine base and/or 2′-H sugar modifications do not lead to significant variations in the thermal stability of the human telomeric sequence (22AG), both in sodium and potassium buffer (Table 1 and Supplementary Figure S4). In order to investigate better this particular property, a thermodynamic study of the thermal denaturation/renaturation of these compounds was performed by DSC and the results are reported in Table 3. The order of ΔH_{cal} and ΔS_{cal} (in absolute terms) for the thermal renaturation of the three species is 22AG-*O* < 22AG-*U* < 22AG. For a renaturation process, high absolute values of ΔH_{cal} favor the stabilization of the structure, but high absolute values of ΔS_{cal} act in the opposite direction. Therefore, the unmodified oligo (22AG) is enthalpically the most favored form but entropically the least favored one. An opposite trend is observed for the 22AG-*O*, while an intermediate situation occurs in the case of the 22AG-*U*. This kind of 'enthalpy–entropy compensation' would explain the similar thermal stability of the three G-quadruplex oligos.

In contrast to their thermal stabilities, differences in the conformation of the 22AG oligos were observed both in sodium and potassium buffer as suggested by the differential spectra in Figure 4a and b. The differential spectra of the 22AG and its *S*- and *U*-analog are similar in shape both in Na^+ and K^+ buffer, denoting a similar spatial organization in the presence of the same ion. However, their conformation in sodium is

quite different from the one in potassium, confirming the essential function of the central cation in the formation of a defined G-quadruplex structure (55). In contrast, the differential spectrum of the 22AG-*O* oligo shows an unusual shape that differs both from the spectra of the other oligos in the same buffer conditions and from one buffer to the other. This supports the hypothesis of an important role of the 2′-position of the sugar moiety in defining the conformational structure of G-quadruplexes, particularly when substitution at this position can hinder the formation of hydrogen bonds.

Enthalpy per quartet

This study, together with previous published values, allows a comparison of the enthalpies per G-quartet between DNA and modified oligomers. Van't Hoff analysis of the melting of an unmodified DNA sample revealed a ΔH^0_{VH} of -19.8, -19.0 and -15.0 kcal/mol quartet for the 15TBA, 18TEL and 22AG samples, respectively (Tables 2 and 3). These values are in fair agreement with the published data (47). In the 15TBA and 18TEL series, phosphorothioates and 2′-*O*-methyl have a similar enthalpy per quartet, whereas the terminal T→U substitution provides a further 9 kcal/mol benefit (Table 2). Concerning parallel quadruplexes, previous analysis of the calorimetric or kinetic (45) data gave a value of -72 kcal mol^{-1} for the TG4 sample (i.e. -18 kcal/mol quartet) in good agreement with enthalpies found for intramolecular quadruplexes (-15 to -20 kcal/mol quartet). More surprising is the very negative ΔH^0_{VH} found for TG4-*R* and TGA-*O* (-124 and -127 kcal mol^{-1}, respectively, corresponding to approximately -30 kcal/mol quartet) (45). These values suggest that the strong stabilizing effect provided by the sugar modification is enthalpic in origin, but only applies to tetramolecular quadruplexes.

CONCLUSION

A systematic thermal analysis of chemically modified G-quadruplex-forming oligonucleotides appears to be indispensable for a better understanding of the subtle features involved in the formation and stabilization of these unique structures. Additionally, the determination of the differential spectra in different buffer conditions may be used as a simple and powerful tool to get more insights into the conformational characteristics of G-quadruplex structures. The results obtained illustrate the necessity of testing several other sequence motifs for identifying additional sequence-dependent effects. Altogether, these findings can be useful for the development of new G-quadruplex-based tools for biomedical, supramolecular chemistry and nanotechnology applications (43).

SUPPLEMENTARY MATERIAL

Supplementary Material is available at NAR Online.

ACKNOWLEDGEMENTS

REFERENCES

1. Keniry,M. (2001) Quadruplex structures in nucleic acids. *Biopolymers*, **56**, 123–146.
2. Neidle,S. and Parkinson,G.N. (2003) The structure of telomeric DNA. *Curr. Opin. Struct. Biol.*, **13**, 275–283.
3. Gellert,M., Lipsett,M.N. and Davies,D.R. (1962) Helix formation by guanylic acid. *Proc. Natl Acad. Sci. USA*, **48**, 2013–2018.
4. Blackburn,E.H. (1994) Telomeres: no end in sight. *Cell*, **77**, 621–623.
5. Sen,D. and Gilbert,W. (1988) Formation of parallel four-stranded complexes by guanine-rich motifs in DNA and its implications for meiosis. *Nature*, **334**, 364–366.
6. Evans,T., Schon,E., Gora-Maslak,G., Patterson,J. and Efstratiadis,A. (1984) S1-hypersensitive sites in eukaryotic promoter regions. *Nucleic Acids Res.*, **12**, 8043–8058.
7. Kilpatrick,M.W., Torri,A., Kang,D.S., Engler,J.A. and Wells,R.D. (1986) Unusual DNA structures in the adenovirus genome. *J. Biol. Chem.*, **261**, 11350–11354.
8. Siddiqui-Jain,A., Grand,C.L., Bearss,D.J. and Hurley,L.H. (2002) Direct evidence for a G-quadruplex in a promoter region and its targeting with a small molecule to repress c-MYC transcription. *Proc. Natl Acad. Sci. USA*, **99**, 11593–11598.
9. Duquette,M.L., Handa,P., Vincent,J.A., Taylor,A.F. and Maizels,N. (2004) Intracellular transcription of G-rich DNAs induces formation of G-loops, novel structures containing G4 DNA. *Genes Dev.*, **18**, 1618–1629.
10. Sundquist,W.I. and Klug,A. (1989) Telomeric DNA dimerizes by formation of guanine tetrads between hairpin loops. *Nature*, **342**, 825–829.
11. Williamson,J.R., Raghuraman,M.K. and Cech,T.R. (1989) Monovalent cation-induced structure of telomeric DNA: the G-quartet model. *Cell*, **59**, 871–880.
12. Frantz,J.D. and Gilbert,W. (1995) A novel yeast gene product, G4p1, with a specific affinity for quadruplex nucleic acids. *J. Biol. Chem.*, **270**, 9413–9419.
13. Bashkirov,V.I., Scherthan,H., Solinger,J.A., Buerstedde,J.M. and Heyer,W.D. (1997) A mouse cytoplasmic exoribonuclease (mXRN1p) with preference for G4 tetraplex substrates. *J. Cell Biol.*, **136**, 761–773.
14. Sun,H., Karow,J.K., Hickson,I.D. and Maizels,N. (1998) The Bloom's syndrome helicase unwinds G4 DNA. *J. Biol. Chem.*, **273**, 27587–27592.
15. Fry,M. and Loeb,L.A. (1999) Human werner syndrome DNA helicase unwinds tetrahelical structures of the fragile X syndrome repeat sequence d(CGG)$_n$. *J. Biol. Chem.*, **274**, 12797–12802.
16. Arimondo,P.B., Riou,J.F., Mergny,J.L., Tazi,J., Sun,J.S., Garestier,T. and Hélène,C. (2000) Interaction of human DNA topoisomerase I with G-quartet structures. *Nucleic Acids Res.*, **28**, 4832–4838.
17. Schaeffer,C., Bardoni,B., Mandel,J.L., Ehresmann,B., Ehresmann,C. and Moine,H. (2001) The fragile X mental retardation protein binds specifically to its mRNA via purine quartet motif. *EMBO J.*, **20**, 4803–4813.
18. Darnell,J.C., Jensen,K.B., Jin,P., Brown,V., Warren,S.T. and Darnell,R.B. (2001) Fragile X mental retardation protein targets G quartet mRNAs important for neuronal function. *Cell*, **107**, 489–499.
19. McEachern,M.J., Krauskopf,A. and Blackburn,E.H. (2000) Telomeres and their control. *Annu. Rev. Genet.*, **34**, 331–358.
20. Zahler,A.M., Williamson,J.R., Cech,T.R. and Prescott,D.M. (1991) Inhibition of telomerase by G-quartet DNA structures. *Nature*, **350**, 718–720.
21. Mergny,J.L. and Hélène,C. (1998) G-quadruplex DNA: a target for drug design. *Nature Med.*, **4**, 1366–1367.
22. Neidle,S. and Read,M.A. (2001) G-quadruplexes as therapeutic targets. *Biopolymers*, **56**, 195–208.
23. Rando,R.F., Ojwang,J., Elbaggari,A., Reyes,G.R., Tinder,R., McGrath,M.S. and Hogan,M.E. (1995) Suppression of human immunodeficiency virus type 1 activity by oligonucleotides which form intramolecular tetrads. *J. Biol. Chem.*, **270**, 1754–1760.
24. Cherepanov,P., Este,J.A., Rando,R.F., Ojwang,J.O., Reekmans,G., Steinfeld,R., David,G., De Clercq,E. and Debyser,Z. (1997) Mode of interaction of G-quartets with the integrase of human immunodeficiency virus type 1. *Mol. Pharmacol.*, **52**, 771–780.
25. Wyatt,J.R., Vickers,T.A., Roberson,J.L., Buckheit,R.W., Klimkait,T., DeBaets,E., Davis,P.W., Rayner,B., Imbach,J.L. and Ecker,D.J. (1994) Combinatorially selected guanosine-quartet structure is a potent inhibitor

of human immunodeficiency virus envelope-mediated cell fusion. *Proc. Natl Acad. Sci. USA*, **91**, 1356–1360.

26. Bates,P.J., Kahlon,J.B., Thomas,S.D., Trent,J.O. and Miller,D.M. (1999) Antiproliferative activity of G-rich oligonucleotides correlates with protein binding. *J. Biol. Chem.*, **274**, 26369–26377.

27. Đapic,V., Bates,P.J., Trent,J.O., Rodger,A., Thomas,S.D. and Miller,D.M. (2002) Antiproliferative activity of G-quartet-forming oligonucleotides with backbone and sugar modifications. *Biochemistry*, **41**, 3676–3685.

28. Shafer,R.H. and Smirnov,I. (2001) Biological aspects of DNA/RNA quadruplexes. *Biopolymers*, **56**, 209–227.

29. Kang,C., Zhang,X., Ratliff,R., Moyzis,R. and Rich,A. (1992) Crystal structure of four-stranded Oxytricha telomeric DNA. *Nature*, **356**, 126–131.

30. Smith,F.W. and Feigon,J. (1993) Strand orientation in the DNA quadruplex formed from the Oxytricha telomere repeat oligonucleotide d(G$_4$T$_4$G$_4$) in solution. *Biochemistry*, **32**, 8682–8692.

31. Đapić,V., Abdomerović,V., Marrington,R., Pederby,J., Rodger,A., Trent,J.O. and Bates,P.J. (2003) Biophysical and biological properties of quadruplex oligodeoxyribonucleotides. *Nucleic Acids Res.*, **31**, 2097–2107.

32. Hardin,C.C., Perry,A.G. and White,K. (2001) Thermodynamic and kinetic characterization of the dissociation and assembly of quadruplex nucleic acids. *Biopolymers*, **56**, 147–194.

33. Bock,L.C., Griffin,L.C., Latham,J.A., Vermaas,E.H. and Toole,J.J. (1992) Selection of single-stranded DNA molecules that bind and inhibit human thrombin. *Nature*, **355**, 564–566.

34. Macaya,R.F., Schultze,P., Smith,F.W., Roe,J.A. and Feigon,J. (1993) Thrombin-binding DNA aptamer forms a unimolecular quadruplex structure in solution. *Proc. Natl Acad. Sci. USA*, **90**, 3745–3749.

35. Padmanabhan,K., Padmanabhan,K.P., Ferrara,J.D., Sadler,J.E. and Tulinsky,A. (1993) The structure of alpha-thrombin inhibited by a 15-mer single stranded DNA aptamer. *J. Biol. Chem.*, **268**, 17651–17654.

36. Kelly,J.A., Feigon,J. and Yeates,T.O. (1996) Reconciliation of the X-ray and NMR structures of the thrombin-binding aptamer d(GGTTGGTGTGGTTGG). *J. Mol. Biol.*, **256**, 417–422.

37. Okazaki,S., Tsuchida,K., Maekawa,H., Ishikawa,H. and Fujiwara,H. (1993) Identification of a pentanucleotide telomeric sequence, (TTAGG)$_n$, in the silkworm *Bombyx mori* and in other insects. *Mol. Cell. Biol.*, **13**, 1424–1432.

38. Wang,Y. and Patel,D.J. (1993) Solution structure of the human telomeric repeat d[AG$_3$(T$_2$AG$_3$)$_3$] G-tetraplex. *Structure*, **1**, 263–282.

39. Parkinson,G.N., Lee,M.P.H. and Neidle,S. (2002) Crystal structure of parallel quadruplexes from human telomeric DNA. *Nature*, **417**, 876–880.

40. Schultze,P., Hud,N.V., Smith,F.W. and Feigon,J. (1999) The effect of sodium, potassium and ammonium ions on the conformation of the dimeric quadruplex formed by the *Oxytricha nova* telomere repeat oligonucleotide d(G(4)T(4)G(4)). *Nucleic Acids Res.*, **27**, 3018–3028.

41. Aboul-ela,F., Murchie,A.I., Norman,D.G. and Lilley,D.M. (1994) Solution structure of a parallel-stranded tetraplex formed by d(TG4T) in the presence of sodium ions by nuclear magnetic resonance spectroscopy. *J. Mol. Biol.*, **243**, 458–471.

42. Phillips,K., Dauter,Z., Murchie,A.I., Lilley,D.M. and Luisi,B. (1997) The crystal structure of a parallel-stranded guanine tetraplex at 0.95 Å resolution. *J. Mol. Biol.*, **273**, 171–182.

43. Davis,J.T. (2004) G-quartets 40 years later: from 5′-GMP to molecular biology and supramolecular chemistry. *Angew. Chem. Int. Ed. Engl.*, **43**, 668–698.

44. Cantor,C.R., Warshaw,M.M. and Shapiro,H. (1970) Oligonucleotide interactions. 3. Circular dichroism studies of the conformation of deoxyoligonucleotides. *Biopolymers*, **9**, 1059–1077.

45. Mergny,J.L., De Cian,A., Ghelab,A., Saccà,B. and Lacroix,L. (2005) Kinetics of tetramolecular quadruplexes. *Nucleic Acids Res.*, **32**, 81–94.

46. Mergny,J.L. and Lacroix,L. (2003) Analysis of thermal melting curves. *Oligonucleotides*, **13**, 515–537.

47. Mergny,J.L., Phan,A.T. and Lacroix,L. (1998) Following G-quartet formation by UV-spectroscopy. *FEBS Lett.*, **435**, 74–78.

48. Alberti,P., Hoarau,M., Guittat,L., Takasugi,M., Arimondo,P.B., Lacroix,L., Mills,M., Teulade-Fichou,M.P., Vigneron,J.P., Lehn,J.M. *et al.* (2002) Triplex vs. quadruplex specific ligands and telomerase inhibition. In Demeunynck,M., Bailly,C. and Wilson,D. (eds), *Small Molecule DNA and RNA Binders: from Synthesis to Nucleic Acid Complexes.* Wiley, VCH Publishers, Weinheim, pp. 315–336.

49. Horvath,M.P. and Schultz,S.C. (2001) DNA G-quartets in a 1.86 Å resolution structure of an *Oxytricha nova* telomeric protein–DNA complex. *J. Mol. Biol.*, **310**, 367–377.

50. Haider,S., Parkinson,G.N. and Neidle,S. (2002) Crystal structure of the potassium form of an *Oxytricha nova* G-quadruplex. *J. Mol. Biol.*, **320**, 189–200.

51. Datta,B., Schmitt,C. and Armitage,B.A. (2003) Formation of a PNA$_2$–DNA$_2$ hybrid quadruplex. *J. Am. Chem. Soc.*, **125**, 4111–4118.

52. Krishnan-Ghosh,Y., Stephens,E. and Balasubramanian,S. (2004) A PNA(4) quadruplex. *J. Am. Chem. Soc.*, **126**, 5944–5945.

53. Liu,H., Kugimiya,A., Sakurai,T., Katahira,M. and Uesugi,S. (2002) A comparison of the properties and the solution structure for RNA and DNA quadruplexes which contain two GGAGG sequences joined with a tetranucleotide linker. *Nucleosides Nucleotides Nucleic Acids*, **21**, 785–801.

54. Randazzo,A., Esposito,V., Ohlenschlager,O., Ramachandran,R. and Mayol,L. (2004) NMR solution structure of a parallel LNA quadruplex. *Nucleic Acids Res.*, **32**, 3083–3092.

55. Balagurumoorthy,P. and Brahmachari,S.K. (1994) Structure and stability of human telomeric sequence. *J. Biol. Chem.*, **269**, 21858–21869.